Finite-Element Analysis of Turbulent Diffusion Flames

Y. M. Kim* and T. J. Chung†
University of Alabama in Huntsville, Huntsville, Alabama

A numerical procedure for the computation of confined, axisymmetric, turbulent diffusion flames is developed. The governing elliptic partial differential equations are solved by the finite-element method to generate the flexible mesh in flow regions with physical and geometrical complexity. This algorithm adopts a sequential velocity-pressure formulation that allows the uncoupling of pressure and velocity. In order to minimize the numerical diffusion, the streamline upwind/Petrov-Galerkin formulation is employed. Turbulence is represented by the k-ϵ model, and the combustion process involves an irreversible one-step reaction at an infinite rate. The time-averaged mixture properties are obtained by weighting the property function with a beta probability density function (pdf). Predictions are made for turbulent reacting and nonreacting flow systems with recirculation, and the results are compared with experimental data.

Nomenclature

a,b = parameter in β function pdf
C_p = specific heat
C_μ = constants in the turbulent model
f = mixture fraction
g = square of fluctuations of mixture fraction
h = enthalpy of mixture
H_{fu} = heat of reaction
k = kinetic energy of turbulence
M = molecular weight
P = pressure
R = universal gas constant
r = distance in radial direction
s = stoichiometric mass of oxidant
T = temperature
u = axial velocity component
v = radial velocity component
W = weighting function
x = axial coordinate distance
β = conserved scalar
ξ = nondimensional mixture fraction
ϵ = rate of dissipation of turbulence energy
μ = molecular viscosity
μ_t = turbulent viscosity
ρ = mixture density
Φ = continuous weighting function
Ψ = discontinuous weighting function

Subscripts

A = airstream
F = fuel stream
fu = fuel
ox = oxidant
pr = product

Superscripts

$'$ = correction
$*$ = estimation

Received Nov. 18, 1987; revision received Aug. 16, 1988.

*Postdoctoral Research Associate, Department of Mechanical Engineering.
†Professor, Department of Mechanical Engineering.

I. Introduction

In many combustion systems, reactants enter in separate streams, oxidizer and fuel being nonpremixed. The resulting turbulent diffusion flames are one of the most challenging topics in engineering sciences. Recently, several studies[1-6] have been carried out with regard to the development of mathematical and numerical modeling for turbulent reacting flows. These studies were motivated by the need for a better understanding of the combustion mechanism in industrial furnaces and propulsive systems such as gas-turbine and ramjet combustors and space shuttle engines. The predictions of the combustor flowfield are desirable not only for understanding and interpretation of experimental data but also for engineering design optimization.

Most of the previous works for turbulent diffusion flames used the finite-difference solution procedures. The basic advantage of the finite-element method is to allow for a flexible mesh. Mapping methods and multiple-grid approaches in the context of finite-difference methods do not provide the same degree of flexibility. For this reason, it is worthwhile to study the application of the finite-element method to turbulent reacting flow.

In the present study, a solution procedure for the analysis of confined, axisymmetric, turbulent diffusion flames is developed. This algorithm adopts a sequential velocity-pressure formulation[7,8] that allows the uncoupling of the pressure and velocity solution. To minimize the numerical diffusion, the streamline upwind/Petrov-Galerkin scheme is employed.[9] Turbulence is represented by the k-ϵ model, which provides an optimal choice between accuracy and economy for most turbulent reacting flows. The one-step forward chemical reaction is assumed to occur at an infinite rate controlled by the mixing of fuel and oxidant streams.[10] The time-averaged mixture properties are obtained by weighting the property functions with a beta probability density function (pdf). Predictions are carried out for the reacting and nonreacting turbulent confined coaxial jets. The computational results are compared with available experimental data.

II. Mathematical Modeling of the Flame Field

A. Mean Flow Equations

In axisymmetric, turbulent reacting flow, the steady-state transport equations of mass, momentum, energy, and mass fraction can be written as

$$\frac{\partial}{\partial x}(\rho u) + \frac{1}{r}\frac{\partial}{\partial r}(\rho v r) = 0 \tag{1}$$

$$\rho u\frac{\partial u}{\partial x}+\rho v\frac{\partial u}{\partial r}-\frac{1}{r}\left[\frac{\partial}{\partial x}\left(r\mu_e\frac{\partial u}{\partial x}\right)+\frac{\partial}{\partial r}\left(r\mu_e\frac{\partial u}{\partial r}\right)\right]$$
$$=-\frac{\partial P}{\partial x}+\frac{1}{r}\left[\frac{\partial}{\partial x}\left(r\mu_e\frac{\partial u}{\partial x}\right)+\frac{\partial}{\partial r}\left(r\mu_e\frac{\partial v}{\partial x}\right)\right]$$
$$-\frac{2}{3}\frac{\partial}{\partial x}\left[\mu_e\left(\frac{\partial u}{\partial x}+\frac{1}{r}\frac{\partial(rv)}{\partial r}\right)\right] \tag{2}$$

$$\rho u\frac{\partial v}{\partial x}+\rho v\frac{\partial v}{\partial r}-\frac{1}{r}\left[\frac{\partial}{\partial x}\left(r\mu_e\frac{\partial v}{\partial x}\right)+\frac{\partial}{\partial r}\left(r\mu_e\frac{\partial v}{\partial r}\right)\right]$$
$$=-\frac{\partial P}{\partial r}+\frac{1}{r}\left[\frac{\partial}{\partial x}\left(r\mu_e\frac{\partial u}{\partial r}\right)+\frac{\partial}{\partial r}\left(r\mu_e\frac{\partial v}{\partial r}\right)\right]$$
$$-2\mu_e\frac{v}{r^2}-\frac{2}{3}\frac{\partial}{\partial r}\left[\mu_e\left(\frac{\partial u}{\partial x}+\frac{1}{r}\frac{\partial(rv)}{\partial r}\right)\right] \tag{3}$$

$$\rho u\frac{\partial f}{\partial x}+\rho v\frac{\partial f}{\partial r}-\frac{1}{r}\left[\frac{\partial}{\partial x}\left(r\mu_f\frac{\partial f}{\partial x}\right)+\frac{\partial}{\partial r}\left(r\mu_f\frac{\partial f}{\partial r}\right)\right]=0 \tag{4}$$

Here, u and v are the time-mean axial and radial velocities, respectively; f is the time-mean mixture fraction, ρ the mean density, and μ_e and μ_f the effective diffusivities.

B. Turbulence Model

The transport equation for turbulence energy k and turbulence energy dissipation ϵ are

$$\rho u\frac{\partial k}{\partial x}+\rho v\frac{\partial k}{\partial r}-\frac{1}{r}\left[\frac{\partial}{\partial x}\left(r\mu_k\frac{\partial k}{\partial x}\right)+\frac{\partial}{\partial r}\left(r\mu_k\frac{\partial k}{\partial r}\right)\right]=G-\rho\epsilon \tag{5}$$

$$\rho u\frac{\partial \epsilon}{\partial x}+\rho v\frac{\partial \epsilon}{\partial r}-\frac{1}{r}\left[\frac{\partial}{\partial x}\left(r\mu_\epsilon\frac{\partial \epsilon}{\partial x}\right)+\frac{\partial}{\partial r}\left(r\mu_\epsilon\frac{\partial \epsilon}{\partial r}\right)\right]$$
$$=C_{\epsilon 1}\frac{\epsilon}{k}G-\frac{C_{\epsilon 2}\rho\epsilon^2}{k} \tag{6}$$

where

$$G=\mu_t\left\{2\left[\left(\frac{\partial u}{\partial x}\right)^2+\left(\frac{\partial v}{\partial r}\right)^2+\left(\frac{v}{r}\right)^2\right]+\left(\frac{\partial u}{\partial r}+\frac{\partial v}{\partial x}\right)^2\right\} \tag{7}$$

The turbulent diffusivities (μ_t, etc.) can be obtained from the turbulent kinetic energy k and the dissipation rate ϵ, such that

$$\mu_t=\rho C_\mu(k^2/\epsilon)$$
$$\mu_e=\mu+\mu_t,\qquad \mu_f=\mu+(\mu_t/\sigma_f)$$
$$\mu_k=\mu+\frac{\mu_t}{\sigma_k},\qquad \mu_\epsilon=\mu+(\mu_t/\sigma_\epsilon) \tag{8}$$

When the flow is reacting, an additional turbulence equation for the concentration fluctuations [$g=\overline{(f-\bar{f})^2}$] is required. Thus,

$$\rho u\frac{\partial g}{\partial x}+\rho v\frac{\partial g}{\partial r}-\frac{1}{r}\left[\frac{\partial}{\partial x}\left(r\mu_g\frac{\partial g}{\partial x}\right)+\frac{\partial}{\partial r}\left(r\mu_g\frac{\partial g}{\partial x}\right)\right]$$
$$=C_{g1}\mu_t\left[\left(\frac{\partial f}{\partial x}\right)^2+\left(\frac{\partial f}{\partial r}\right)^2\right]-C_{g2}\rho\epsilon\frac{g}{k} \tag{9}$$

in which $\mu_g=\mu+(\mu_t/\sigma_g)$. The values of the model constants are given in Table 1.

C. Combustion Models

In physically controlled diffusion flames, it is assumed that the chemistry is sufficiently fast and that intermediate species do not play a significant role. The reaction takes place in an irreversible, single step as follows:

$$\text{oxidizer}+\text{fuel}\rightarrow\text{product}$$

For fast chemistry and the one-step irreversible reaction, there will be no oxidant present for mixtures richer than stoichiometric and no fuel present when the mixture is weaker than stoichiometric. Both will be zero when the mixture is stoichiometric.

In a two-feed system, the mixture fraction at any point is defined by

$$\xi\equiv(\beta-\beta_A)/(\beta_F-\beta_A) \tag{10}$$

where

$$\beta\equiv Y_{\text{fu}}-Y_{\text{ox}}/s \tag{11}$$

Here, Y_{fu} and Y_{ox} denote the mass fractions of fuel and oxidizer, respectively; s is the stoichiometric oxidant required to burn 1 kg fuel, β_F and β_A are the values of the conserved scalar β at the inlet, and the subscripts A and F denote the air and fuel stream conditions at the inlet.

The assumption of chemical equilibrium is now made, so that

$$0\le\xi\le\xi_{\text{st}}:\qquad Y_{\text{fu}}=0,\qquad Y_{\text{ox}}=Y_{\text{ox},A}\frac{\xi_{\text{st}}-\xi}{\xi_{\text{st}}} \tag{12}$$

$$\xi_{\text{st}}\le\xi\le 1:\qquad Y_{\text{ox}}=0,\qquad Y_{\text{fu}}=Y_{\text{fu},F}\frac{\xi-\xi_{\text{st}}}{\xi_{\text{st}}} \tag{13}$$

with

$$\xi_{\text{st}}=Y_{\text{ox},A}/(sY_{\text{fu},F}+Y_{\text{ox},A}) \tag{14}$$

The mass fraction of the products can be obtained by the mass conservation:

$$Y_{\text{pr}}=1.0-(Y_{\text{ox}}+Y_{\text{fu}}) \tag{15}$$

Furthermore, the property functions for the mixture can be expressed by the mixture fraction. For an adiabatic flow, we have

$$h(\xi)=\xi h_f+(1-\xi)h_A \tag{16}$$

$$\int_0^T\bar{C}_p\,dT=h(\xi)-Y_{\text{fu}}H_{\text{fu}} \tag{17}$$

$$\bar{C}_p(\xi)=\sum_i Y_i(\xi)C_{pi}(\xi) \tag{18}$$

$$\rho(\xi)=M(\xi)P/RT(\xi) \tag{19}$$

and

$$\frac{1}{M(\xi)}=\frac{Y_{\text{fu}}(\xi)}{M_{\text{fu}}}+\frac{Y_{\text{ox}}(\xi)}{M_{\text{ox}}}+\frac{Y_{\text{pr}}(\xi)}{M_{\text{pr}}} \tag{20}$$

where H, T, C_p, ρ, and H_{fu} are the enthalpy, temperature, specific heat, density of the mixture, and the heat of reaction, respectively.

From the preceding relations, the instantaneous thermochemical state is related to the instantaneous value of the

Table 1 Values of constants for the turbulence model

C_μ	$C_{\epsilon 1}$	$C_{\epsilon 2}$	C_{g1}	C_{g2}	σ_k	σ_ϵ	σ_f	σ_g
0.09	1.44	1.92	2.8	2.0	1.0	1.3	0.6	0.6

mixture fraction. However, the fluctuation properties should be considered to take account of the effect of turbulent eddies on thermochemical properties. The most convenient way of achieving this is via the introduction of the probability density function $P(\xi,x_i)$. This function contains the information of both mean and fluctuation quantities of the mixture fraction. In the present study, the time-mean properties of the reacting mixture are evaluated by convoluting the property functions with a beta probability density distribution. Any mean mixture property ϕ is evaluated from the expression $\bar{\phi}$

$$\bar{\phi} = \int_0^1 \phi(\xi) P(\xi,x_i)\, d\xi \tag{21}$$

$$P(\xi,x_i) = \frac{\xi^{a-1}(1-\xi)^{b-1}}{\int_0^1 \xi^{a-1}(1-\xi)^{b-1}\, d\xi}$$

$$a = f\left[\frac{f(1-f)}{g} - 1\right]$$

$$b = (1-f)\left[\frac{f(1-f)}{g} - 1\right] \tag{22}$$

From the definition of the Favre averaging, $\tilde{\phi} = \overline{\rho\phi}/\bar{\rho}$, the Favre average of the inverse density equals the inverse of the Reynolds average of the density $[1/\bar{\rho} = (\widetilde{1/\rho})]$. Using this relation, the mean density may be obtained from

$$\bar{\rho}(x_i) = \left[\int_0^1 \frac{1}{\rho(\xi)} P(\xi,x_i)\, d\xi\right]^{-1} \tag{23}$$

With these properties of the proposed combustion model involved in turbulence together with the mean flow equations, we discuss the detailed solution procedure in the following section.

III. Segregated Velocity-Pressure Formulation

To treat the coupling of the velocity-pressure field, the segregated velocity-pressure formulation is employed. The sequential algorithm of the finite-element method[7,8] is similar to the SIMPLE algorithm of the finite-difference method.[11] All transport equations are solved by using the implicit quasi-unsteady algorithm of the finite-element method.[12]

The momentum equations can be solved only when the pressure field is estimated or given. Unless the correct pressure field is employed, the resulting velocity field will not satisfy the continuity equations. At this point, the corrected pressure P is decomposed into a best estimate P^* and a pressure correction term P' as follows:

$$P = P^* + P' \tag{24}$$

The corresponding velocity corrections u' and v' can be introduced in a similar manner as

$$u = u^* + u', \qquad v = v^* + v' \tag{25}$$

With the help of this decomposition, the following expressions can be derived for the estimated velocities (u^*,v^*), the velocity corrections (u',v'), and the pressure correction (P'):

Estimated velocity field (u^*,v^*):

$$\rho\frac{\partial u^*}{\partial t} = \frac{1}{r}\left[\frac{\partial}{\partial x}\left(r\mu_e\frac{\partial u^*}{\partial x}\right) + \frac{\partial}{\partial r}\left(r\mu_e\frac{\partial u^*}{\partial r}\right)\right] - \rho\left(u^n\frac{\partial u^*}{\partial x} + v^n\frac{\partial v^*}{\partial r}\right) + S^{u*} \tag{26}$$

$$\rho\frac{\partial v^*}{\partial t} = \frac{1}{r}\left[\frac{\partial}{\partial x}\left(r\mu_e\frac{\partial v^*}{\partial x}\right) + \frac{\partial}{\partial r}\left(r\mu_e\frac{\partial v^*}{\partial r}\right)\right] - \rho\left(u^n\frac{\partial v^*}{\partial x} + v^n\frac{\partial v^*}{\partial r}\right) + S^{v*} \tag{27}$$

Velocity corrections (u',v'):

$$\rho\frac{\partial u'}{\partial t} = -\frac{\partial P'}{\partial x} \tag{28}$$

$$\rho\frac{\partial v'}{\partial t} = -\frac{\partial P'}{\partial r} \tag{29}$$

Pressure correction (P'):

$$\frac{1}{r}\left[\frac{\partial}{\partial x}\left(r\frac{\partial P'}{\partial x}\right) + \frac{\partial}{\partial r}\left(r\frac{\partial P'}{\partial r}\right)\right] \cong \frac{R^*}{\Delta t} \tag{30}$$

where Δt is the time interval used in computation, and

$$S^{u*} = -\frac{\partial P^n}{\partial x} + \frac{1}{r}\left[\frac{\partial}{\partial x}\left(r\mu_e\frac{\partial u^n}{\partial x}\right) + \frac{\partial}{\partial r}\left(r\mu_e\frac{\partial v^n}{\partial x}\right)\right] - \frac{2}{3}\frac{\partial}{\partial x}\left[\mu_e\left(\frac{\partial u^n}{\partial x} + \frac{1}{r}\frac{\partial(rv^n)}{\partial r}\right)\right] \tag{31}$$

$$S^{v*} = -\frac{\partial P^n}{\partial r} + \frac{1}{r}\left[\frac{\partial}{\partial x}\left(r\mu_e\frac{\partial v^n}{\partial r}\right) + \frac{\partial}{\partial r}\left(r\mu_e\frac{\partial v^n}{\partial r}\right)\right] - 2\mu_e\frac{v^n}{r^2} - \frac{2}{3}\frac{\partial}{\partial r}\left[\mu_e\left(\frac{\partial u^n}{\partial x} + \frac{1}{r}\frac{\partial(rv^n)}{\partial r}\right)\right] \tag{32}$$

$$R^* = \frac{\partial}{\partial x}(\rho u^*) + \frac{1}{r}\frac{\partial}{\partial r}(\rho r v^*) \tag{33}$$

Here, the superscript n denotes the previous time step.

Finally, the overall sequential solution procedure is outlined below:

1) Guess the values of all the variables including the pressure field P^*.

2) Calculate auxiliary variables such as temperature, density, etc., from the associated combustion model.

3) Solve the axial and radial momentum equations for the estimated velocity components.

4) Calculate the pressure corrections that enforce the continuity.

5) Calculate the pressure and the corrected velocities.

6) Solve the transport equations for other variables (i.e., k, ϵ, f, g).

7) Treat the new values of the variables as improved guesses, and return to step 2 and repeat the process until convergence.

IV. Streamline Upwind/Petrov-Galerkin Formulation

The streamline upwind/Petrov-Galerkin scheme[9] is employed to solve the advection-diffusion problems. Unlike the standard Galerkin weighted residual method, the streamline upwind/Petrov-Galerkin formulation requires discontinuous weighting functions of the form

$$W = \Phi + \Psi \tag{34}$$

where Φ denotes a continuous weighting function, and Ψ represents the discontinuous streamline upwind contribution. Both Φ and Ψ are assumed to be smooth on the element interiors.

Using the streamline upwind/Petrov-Galerkin method, the momentum equations can be written in matrix form as

$$\left(\frac{A_{\alpha\beta}}{\Delta t} + B_{\alpha\beta} + C_{\alpha\beta}\right)u^*_\beta = \frac{A_{\alpha\beta}}{\Delta t}u^n_\beta - D_\alpha \tag{35}$$

$$\left(\frac{A_{\alpha\beta}}{\Delta t} + B_{\alpha\beta} + C_{\alpha\beta}\right)v^*_\beta = \frac{A_{\alpha\beta}}{\Delta t}v_\beta - E_\alpha \tag{36}$$

in which

$$A_{\alpha\beta} = \int_\Omega r\rho W_\alpha \Phi_\beta \, d\Omega \tag{37}$$

$$B_{\alpha\beta} = \int_\Omega r\mu_e\left(\frac{\partial\Phi_\alpha}{\partial x}\frac{\partial\Phi_\beta}{\partial x} + \frac{\partial\Phi_\alpha}{\partial r}\frac{\partial\Phi_\beta}{\partial r}\right) d\Omega \tag{38}$$

$$C_{\alpha\beta} = \int_\Omega r\rho W_\alpha\left(u^n\frac{\partial\Phi_\beta}{\partial x} + v^n\frac{\partial\Phi_\beta}{\partial r}\right) d\Omega \tag{39}$$

$$\begin{aligned} D_\alpha = {} & \int_\Omega r\mu_e\left(\frac{\partial\Phi_\alpha}{\partial x}\frac{\partial u^n}{\partial x} + \frac{\partial\Phi_\alpha}{\partial r}\frac{\partial v^n}{\partial x}\right) d\Omega \\ & - \frac{2}{3}\int_\Omega r\frac{\partial\Phi_\alpha}{\partial x}\mu_e\left(\frac{\partial u^n}{\partial x} + \frac{\partial v^n}{\partial r} + \frac{v^n}{r}\right) d\Omega \\ & + \int_\Omega rW_\alpha\frac{\partial P}{\partial x}\, d\Omega - \int_\Gamma rW_\alpha\tau_x \, d\Gamma \end{aligned} \tag{40}$$

$$\begin{aligned} E_\alpha = {} & \int_\Omega r\mu_e\left(\frac{\partial\Phi_\alpha}{\partial x}\frac{\partial u^n}{\partial x} + \frac{\partial\Phi_\alpha}{\partial r}\frac{\partial v^n}{\partial r}\right) d\Omega \\ & + 2\int_\Omega \mu_e W_\alpha\frac{v^n}{r}\, d\Omega - \frac{2}{3}\int_\Omega\left(r\frac{\partial\Phi_\alpha}{\partial r} + W_\alpha\right) \\ & \times \mu_e\left(\frac{\partial u^n}{\partial x} + \frac{\partial v^n}{\partial r} + \frac{v^n}{r}\right) d\Omega + \int_\Omega rW_\alpha\frac{\partial P}{\partial r}\, d\Omega \\ & - \int_\Gamma r\Phi_\alpha\tau_r \, d\Gamma \end{aligned} \tag{41}$$

By calculating the coefficients (u^n, v^n, etc.) at the previous time step, the system of Eqs. (35) and (36) is linearized, and the solution procedure is made noniterative within each step. Since the diffusion terms are treated implicitly in this Euler backward scheme, there are no instabilities connected with the diffusive limit for explicit time-integration algorithms. If steady-state solutions are of interest, the time step may be as large as allowed by the linear advective-diffusive limits.[9,13]

The pressure correction equations can be discretized as

$$F_{\alpha\beta}P'_\beta + G_\alpha = 0 \tag{42}$$

where

$$F_{\alpha\beta} = \int_\Omega r\left(\frac{\partial\Phi_\alpha}{\partial x}\frac{\partial\Phi_\beta}{\partial x} + \frac{\partial\Phi_\alpha}{\partial r}\frac{\partial\Phi_\beta}{\partial r}\right) d\Omega \tag{43}$$

$$G_\alpha = \frac{1}{\Delta t}\int_\Omega r\Phi_\alpha\left[\frac{\partial}{\partial x}(\rho u^*) + \frac{1}{r}\frac{\partial}{\partial r}(r\rho v^*)\right] d\Omega \tag{44}$$

The velocity correction equations (u',v') are discretized as

$$M_{\alpha\beta}\dot{u}'_\beta = -H^{(u)}_\alpha \tag{45}$$

$$M_{\alpha\beta}\dot{v}'_\beta = -H^{(v)}_\alpha \tag{46}$$

with

$$\dot{u}'_\beta = \frac{u^{(n+1)}_\beta - u^*_\beta}{\Delta t}, \qquad \dot{v}'_\beta = \frac{v^{(n+1)}_\beta - v^*_\beta}{\Delta t} \tag{47}$$

$$M_{\alpha\beta} = \int_\Omega r\rho\Phi_\alpha\Phi_\beta \, d\Omega \tag{48}$$

$$H^{(u)}_\alpha = \int_\Omega r\Phi_\alpha\frac{\partial P'}{\partial x}\, d\Omega \tag{49}$$

$$H^{(v)}_\alpha = \int_\Omega r\Phi_\alpha\frac{\partial P'}{\partial r}\, d\Omega \tag{50}$$

In addition, the turbulent transport equations (k, ϵ) may be discretized such that

$$\left(\frac{A_{\alpha\beta}}{\Delta t} + B^{(k)}_{\alpha\beta} + C_{\alpha\beta}\right)k^{(n+1)}_\beta = \frac{A_{\alpha\beta}}{\Delta t}k^n_\beta - H^{(k)}_\alpha \tag{51}$$

$$\left(\frac{A_{\alpha\beta}}{\Delta t} + B^{(\epsilon)}_{\alpha\beta} + C_{\alpha\beta}\right)\epsilon^{(n+1)}_\beta = \frac{A_{\alpha\beta}}{\Delta t}\epsilon^n_\beta - H^{(\epsilon)}_\alpha \tag{52}$$

where

$$B^{(k)}_{\alpha\beta} = \frac{1}{\sigma_k}B_{\alpha\beta} + C_\mu\int_\Omega r\rho^2\frac{k^n}{\mu_t}W_\alpha\Phi_\beta \, d\Omega \tag{53}$$

$$B^{(\epsilon)}_{\alpha\beta} = \frac{1}{\sigma_\epsilon}B_{\alpha\beta} + C_{\epsilon 2}\int_\Omega r\rho\frac{\epsilon^n}{k^n}W_\alpha\Phi_\beta \, d\Omega \tag{54}$$

$$H^{(k)}_\alpha = -\int_\Omega rW_\alpha G \, d\Omega \tag{55}$$

$$H^{(\epsilon)}_\alpha = -C_{\epsilon 1}\int_\Omega rW_\alpha\frac{\epsilon^n}{k^n}G \, d\Omega \tag{56}$$

The transport equations for the mixture fraction f and concentration fluctuations g are discretized as

$$\left(\frac{A_{\alpha\beta}}{\Delta t} + \frac{1}{\sigma_f}B_{\alpha\beta} + C_{\alpha\beta}\right)f^{(n+1)}_\beta = \frac{A_{\alpha\beta}}{\Delta t}f^n_\beta \tag{57}$$

$$\left(\frac{A_{\alpha\beta}}{\Delta t} + B^{(g)}_{\alpha\beta} + C_{\alpha\beta}\right)g^{(n+1)}_\beta = \frac{A_{\alpha\beta}}{\Delta t}g^n_\beta + H^{(g)}_\alpha \tag{58}$$

where

$$B^{(g)}_{\alpha\beta} = \frac{1}{\sigma_g}B_{\alpha\beta} + C_{g2}\int_\Omega W_\alpha\Phi_\beta r\rho\frac{\epsilon^n}{k^n}\, d\Omega \tag{59}$$

$$S^{(g)}_\alpha = C_{g1}\int_\Omega W_\alpha r\mu_t\left\{\left(\frac{\partial f^n}{\partial x}\right)^2 + \left(\frac{\partial f^n}{\partial r}\right)^2\right\} d\Omega \tag{60}$$

For the streamline upwind/Petrov-Galerkin weak forms of Eqs. (35) and (36), general boundary conditions are u or τ_x and v or τ_r, specified as

$$\tau_x = n_r\left(\frac{\partial v}{\partial x} + \frac{\partial u}{\partial r}\right)\mu_e + n_x\left(2\frac{\partial u}{\partial x} - \frac{2}{3}Q\right)\mu_e \tag{61}$$

$$\tau_r = n_r\left(2\frac{\partial v}{\partial r} - \frac{2}{3}Q\right)\mu_e + n_x\left(\frac{\partial v}{\partial x} + \frac{\partial u}{\partial r}\right)\mu_e \tag{62}$$

with

$$Q = \frac{\partial u}{\partial r} + \frac{1}{r}\frac{\partial(rv)}{\partial r}$$

where n_x and n_r are the direction cosines of the outward normal to the boundary Γ.[13] For the streamline upwind/Petrov-Galerkin weak form of other scalar variables ϕ (i.e., k, ϵ, f, and g), general boundary conditions are simply ϕ or $\partial\phi/\partial n$ specified on Γ.

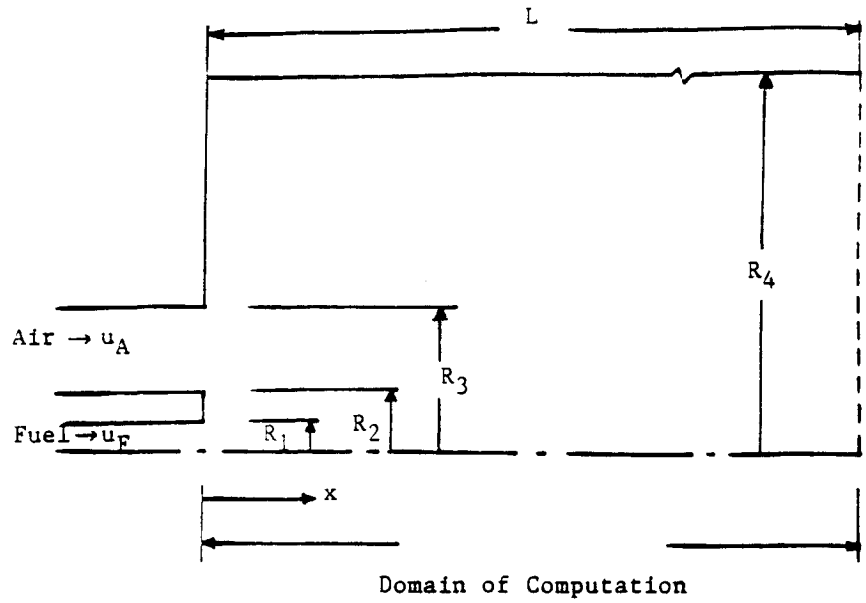

Fig. 1 Geometry of coaxial jets in a sudden expansion.

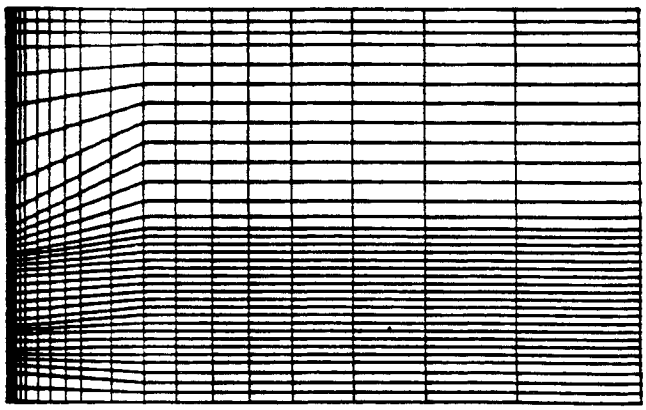

Fig. 2 Finite-element mesh for a confined coaxial jet.

Table 2 Inlet conditions for confined coaxial jets configurations

	Nonreacting flow	Reacting flow
Stoichiometric A/F ratio	—	10.6
Inlet A/F ratio	—	15.75
Heat of reaction, J/kg of reactant	—	2.63×10^7
Inlet fuel velocity u_F, m/s	5.0	21.57
Inlet air velocity u_A, m/s	15.0	13.46
Inlet fuel density ρ_F, kg/m^3	1.0	1.6
Inlet air density ρ_A, kg/m^3	1.0	0.474
Fuel side inner radius R_1, m	0.00805	0.010
Fuel side outer radius R_2, m	0.01080	0.022
Air side inner radius R_3, m	0.02250	0.039
Outlet radius R_4, m	0.06240	0.105
Combustor length L, m	0.59500	0.900

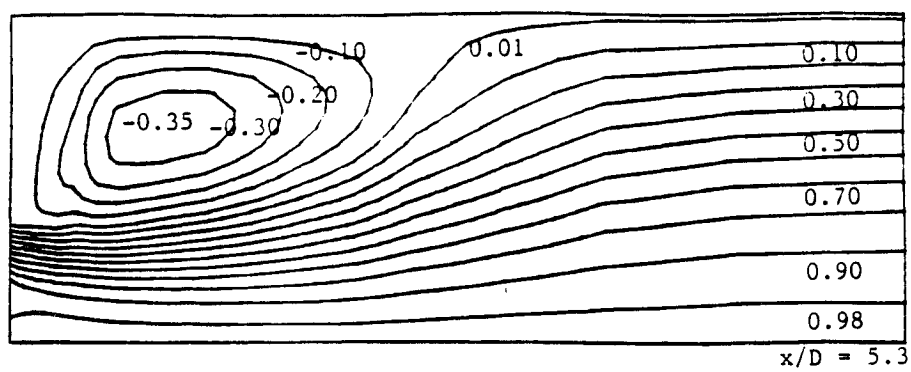

Fig. 3 Streamlines in a confined coaxial jet; the predicted recirculation length (3.1D) is somewhat less than the measured values (3.28D) of Habib and Whitelaw.[15]

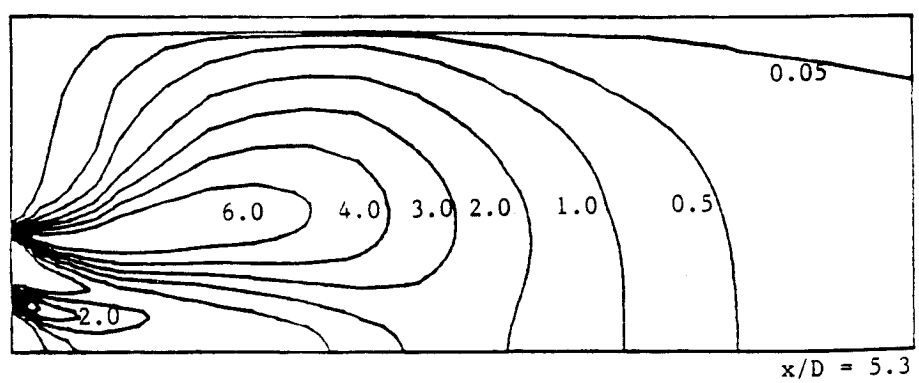

Fig. 4 Contours of turbulent kinetic energy in a confined coaxial jet; the large variation of kinetic energy occurs mainly at the edge of the recirculation zone and the mixing layer region for $x \leq 2$.

For the inlet to the coaxial jet, u, v, k, ϵ, f, and g are all specified. The turbulent kinetic energy is specified by experimental data or reasonable profiles. Since no measurements are available for the length scale, the following expression is used for the calculation of the dissipation rate:

$$\epsilon = C_\mu k^{3/2}/0.03D_h \tag{63}$$

where D_h is the hydraulic diameter.

The mixture fraction at the inlet stream is known by definition ($f = 0.0$, $f_F = 1.0$), and thus the fluctuations g of the mixture fraction are by definition zero for the inlet of the oxidizer and fuel side. At outlet boundaries, traction free boundary conditions ($\tau_x = \tau_r = 0$) or ($\tau_x = v = 0$) are used with $\partial\phi/\partial n = 0$. At symmetry, the normal gradients of all scalar variables ($\partial\phi/\partial n$) are zero, and the radial velocity component v and tangential surface traction τ_x are zero.

The wall regions present several flow characteristics that distinguish them from the other regions of the flow, such as steep gradients and a relatively low level of turbulence. To account for flow phenomena in wall regions, the wall function method is commonly employed.[14] In the context of finite elements, the wall-function method can be implemented by assuming a constant shear stress up to a distance δ within the near-wall region of the flow. With this assumption, the shear stress is calculated by the modified log law

$$|\tau_w| = \rho\kappa u_\tau C_\mu^{1/4} k^{1/2}/\ell_m E\delta^+ \tag{64}$$

with

$$\delta^+ = \rho\delta(C_\mu^{1/2}k)^{1/2}/\mu \tag{65}$$

in which u_τ and k are the potential values computed at the previous time step. Once the near-wall values of the shear stresses are evaluated, near-wall values of ϵ can be calculated

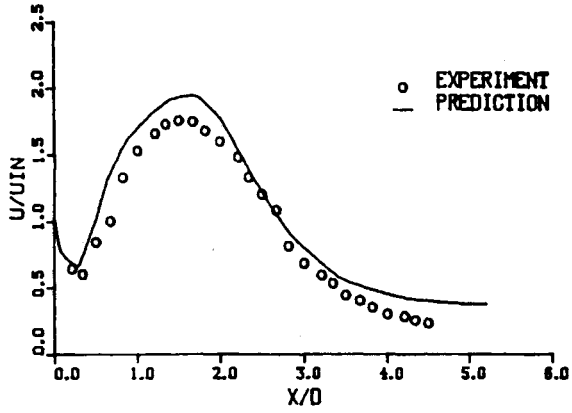

Fig. 5 Axial velocity profile along the centerline in a confined coaxial jet; there is a tendency to overprediction for the centerline axial velocity. The overprediction for coaxial jets may stem from the incorrect representation of the turbulent-diffusion process.

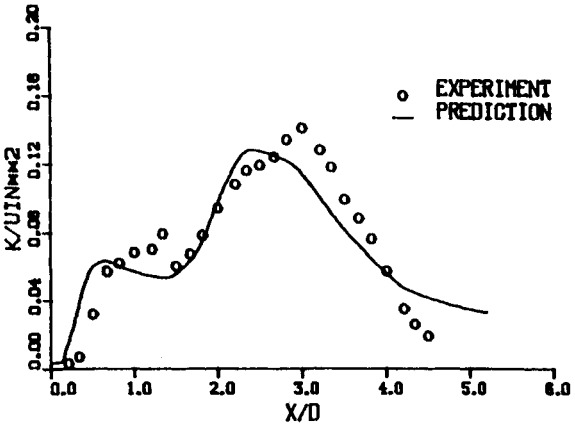

Fig. 6 Axial profile of turbulent kinetic energy along the centerline in a confined coaxial jet; the turbulent kinetic energy is qualitatively well predicted, but the apparent deviation exists with experimental data. The reason for this deviation could be tied into the overprediction in axial velocity.

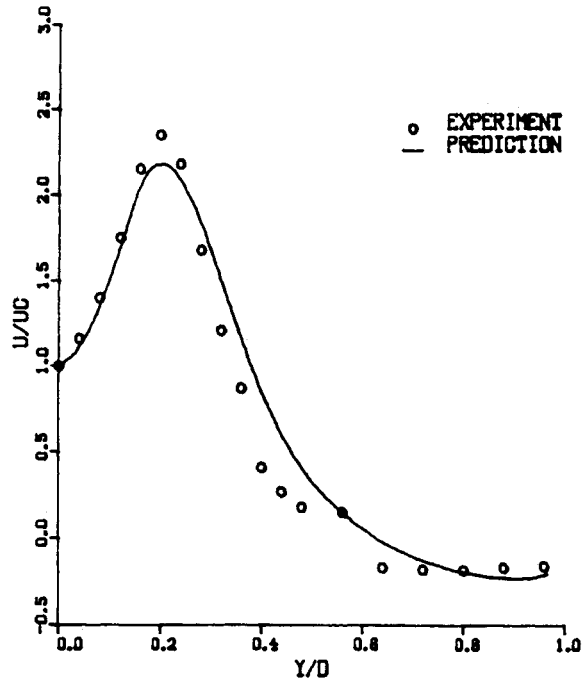

Fig. 7a Radial profiles of axial velocity in a confined coaxial jet ($x/D = 0.616$); the predicted axial velocities are in qualitative agreement with the experimental data.

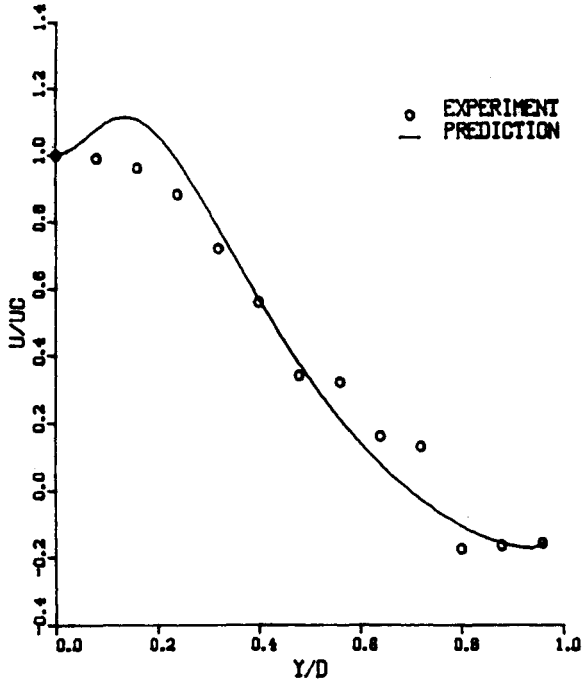

Fig. 7b Radial profiles of axial velocity in a confined coaxial jet (x/D = 1.43); the predicted axial velocities are in qualitative agreement with the experimental data.

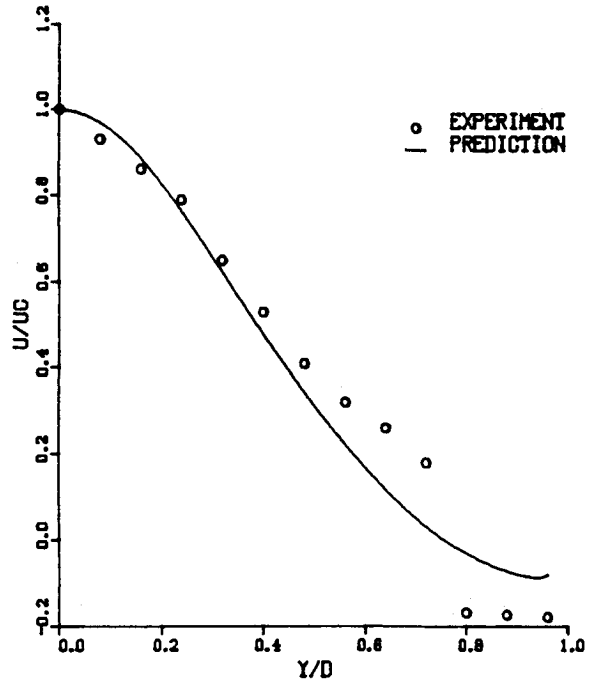

Fig. 7c Radial profiles of axial velocity in a confined coaxial jet (x/D = 2.23); the predicted axial velocities are in qualitative agreement with the experimental data, except the recirculating flow region.

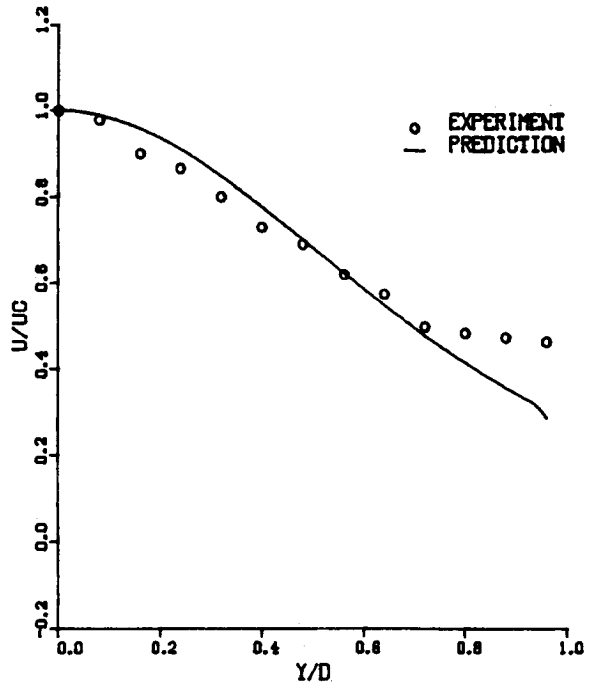

Fig. 7d Radial profiles of axial velocity in a confined coaxial jet ($x/D = 3.67$); the predicted axial velocities are in qualitative agreement with the experimental data, except the near-wall region.

from

$$\epsilon = |\tau_w/\rho|^{3/2}/\kappa\delta \tag{66}$$

V. Discussion

The flow of confined coaxial jets is an idealized representation of the gas-turbine combustor with two streams representing fuel and oxidant flows. The mixing of the two streams is important to the combustion efficiency and the pollutant formation. The geometry of coaxial turbulent reacting and nonreacting flow is shown in Fig. 1. The flow parameters and the geometric dimensions are listed in Table 2.

A. Confined Turbulent Coaxial Jets

Calculations have been made for geometrical parameters corresponding to experiments of Habib and Whitelaw.[15] In this study, we have considered only the case with a velocity ratio of 3.0. To provide boundary conditions at the inlet, the uniform distribution is used for u, together with $v = 0$. Constant values ($k = 0.005u^2$) are assumed for the turbulent kinetic energy profile. Inlet values for ϵ are estimated from Eq. (63). The initial flowfield is assumed to be uniform, and the turbulence quantitites are given simplistic distributions based on constant turbulent kinetic energy and constant length scale.

The finite-element mesh arrangement for the confined coaxial jets is shown in Fig. 2. The irregular grids are generated in order to improve the aspect ratios and to optimize the mesh arrangement. The general flow characteristics are shown in Figs. 3 and 4, where streamlines and kinetic energy contours are represented. In Fig. 3, the length of the recirculation zone is $3.1D$. This is somewhat less than the measured value ($3.28D$). In Fig. 4, the large variation of kinetic energy occurs mainly at the edge of the recirculation zone and the mixing-layer region for $x/D \leq 2$, whereas the low level of turbulent kinetic energy and its small variation occur at the core region. Figures 5 and 6 present the profiles of axial velocity and turbulent kinetic energy along the centerline. The predictions show an initial decrease in the centerline velocity, indicating an initial entrainment of the central jet by the high-velocity outstream. Then the velocity increases as the outer stream spreads into and mixes with the inner stream.

After reaching a peak at $x = 1.7D$, the predicted velocity decays toward the developed profile for downstream. It can be seen that there is a tendency to overprediction for the centerline axial velocity. The overprediction for the coaxial jets with a velocity ratio of 3 may stem from the assumed inlet conditions, the wall function, and the incorrect representation of the turbulent diffusion process. In Fig. 6, the turbulent kinetic energy is qualitatively well predicted. But the apparent deviation exists with the experimental data. The reason for this deviation could be tied into the overprediction in axial velocity. Figures 7a–7d show the comparison of predicted and measured radial profiles of axial velocity at various downstream stations. It can be seen from Figs. 7a–7d that the profiles agree qualitatively at all stations.

B. Confined Turbulent Diffusion Flame

A number of earlier studies[1,3,4] have been concerned with the measurement of mean flow properties of axisymmetric

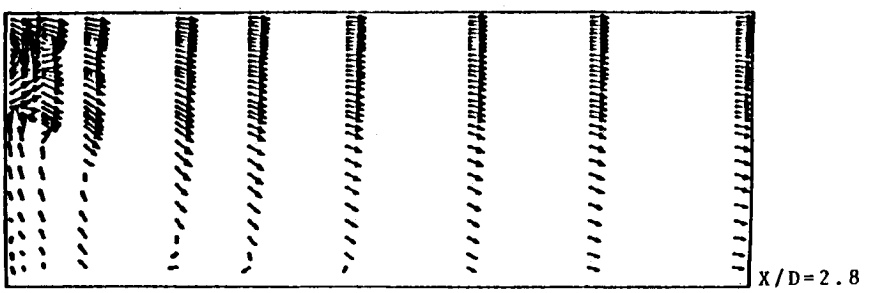

Fig. 8 Velocity vectors of turbulent diffusion flames in a cylindrical combustion chamber ($F/A = 0.0635$, $Re = 16{,}300$); the flow pattern with turbulent mixing and recirculation is shown, with the length of recirculation being approximately $1.4D$.

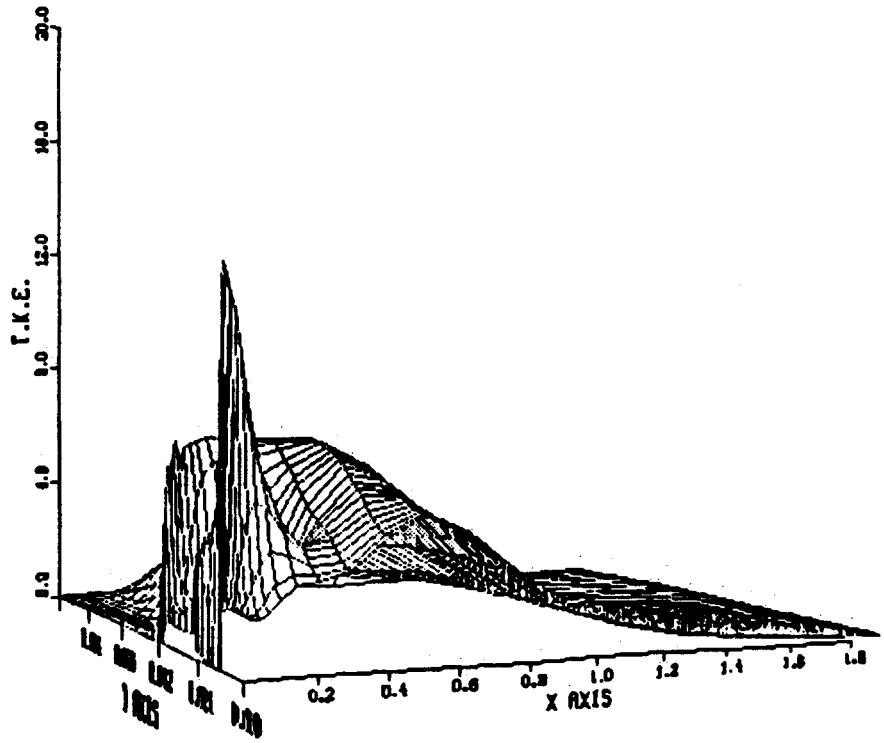

Fig. 9 Spatial distribution of turbulent kinetic energy in a confined diffusion flame ($F/A = 0.0635$); the largest variation occurs at an axial position of $0.6D$ and a radial position of $0.07D$; the second largest variation occurs mainly at the edge of the recirculation zone.

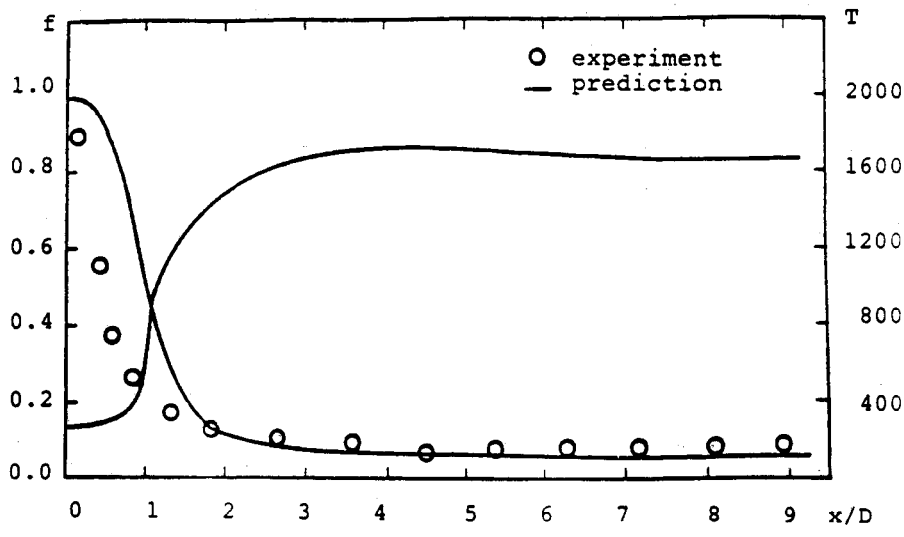

Fig. 10 Axial variation of mixture fraction and temperature in a turbulent diffusion flame ($F/A = 0.0635$); the predicted values of the mixture fraction have the same qualitative trends as do the experimental values (Lockwood et al.[1]). However, significant quantitative differences exist; close to the inlet where the gradients in both axial and radial directions are steep, the measurements exhibit a faster axial decay rate than do the predictions.

confined diffusion flames. In the present study, the geometry of Lockwood et al.[1] is selected for purposes of demonstrating the calculation procedure. In a two-feed system, the fuel and air are entered as coaxial jets into a suddenly expanding chamber. The flame is stabilized at the dividing lip between the two streams. In the present study, the flame field is calculated for a fuel-air ratio of 0.0635. The test condition for the prediction is given in Table 2.

The turbulent reacting flow calculations are started by using the uniform cold-flow conditions. In solving the turbulent reacting flow, underrelaxation procedures are employed for better numerical stability. The underrelaxation factors for k and ϵ are 0.8; density and turbulent viscosity are underrelaxed by 0.6 and 0.5.

The flow pattern with turbulent mixing and recirculation is shown in Fig. 8. The length of the recirculation zone is approximately $1.4D$, and this is somewhat longer than the finite-difference result.[3] Figure 9 shows the spatial variation of turbulent kinetic energy. The largest variation of turbulent kinetic energy occurs at an axial distance of $0.6D$ from the inlet and a radial position of $0.07D$; the second largest variation occurs mainly at the edge of the recirculation zone. As would be expected, these zones are located where the velocity gradient is large and the mean velocity small.

In Fig. 10, the predicted axial profiles of the mixture fraction and temperature are presented. The predicted values of the mixture fraction have the same qualitative trends as the experimental data.[1] It can be seen that, close to the inlet where

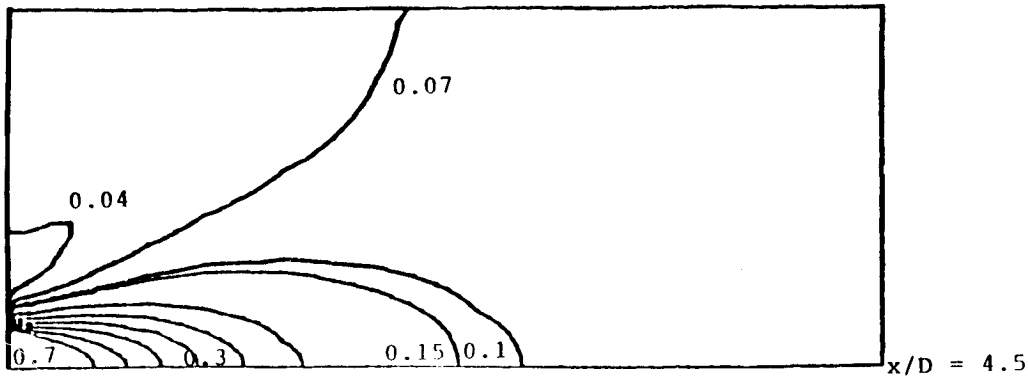

Fig. 11 Contours of mixture fraction in a turbulent diffusion flame (F/A = 0.0635); the predicted contour lines of the mixture fraction have the same qualitative trends as the experimental values (Lockwood et al.[1]).

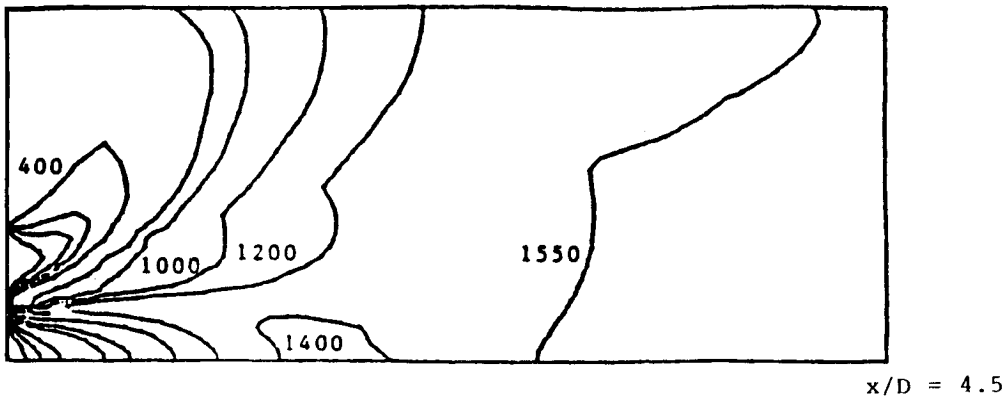

Fig. 12 Contours of temperature in a turbulent diffusion flame (F/A = 0.0635); at the mixing region near the inlet, the temperature rises quickly at some distance downstream and the flame front is developed.

the gradients in both the axial and radial distributions are steep, the measurements exhibit a faster axial decay rate than do the predictions. Figures 11 and 12 illustrate the contours of the time-mean mixture fraction and the time-mean temperature, respectively. As can be seen in Fig. 12, at the mixing region near the inlet, the temperature rises quickly at some distance downstream, and the flame front is developed. At the centerline, the high temperature is maintained. This indicates that the centerline is completely inside the flame. At the wall, the temperature rises sharply as the flame spreads to the wall.

In summary, we comment that turbulence modeling is one thing and numerical simulation of such modeling is quite another. Still another endeavor is the experimental measurements. First of all, the turbulence modeling must represent the correct physical behavior. Then the numerical analysis is only as good as the physical model. Often, errors involved in experimental measurements may bring in further confusion. The apparent deviation between the predictions and measurements may stem from the incorrect representation of the turbulent diffusion process, the treatment of the wall function, and the assumed inlet conditions, provided that the experimental measurements are correct. It is quite possible that the eddy viscosity turbulence model such as the one used here may be inadequate for turbulent diffusion in flows with strong streamline curvatures. This may be regarded as the cause for disagreements between the prediction and experimental measurements. The strength of the present finite-element formulation herein lies in the favorable features such as minimal numerical diffusion, accurate boundary representation of complex geometry, and adaptive local refinement with unstructured grids.

VI. Conclusion

The finite-element algorithm for the computation of confined, axisymmetric, turbulent diffusion flames is developed. Predictions are made for the turbulent reacting and nonreacting flow system with recirculation, and the numerical results are compared with available experimental data. The proposed finite-element procedure exhibits the ability to predict the variable-viscosity/variable-density flow in the turbulent flame field.

The strength of the present finite-element formulation herein lies in the favorable features such as minimal numerical diffusion, accurate boundary representation of complex geometry, and adaptive local refinement with unstructured grids. This is the area to which the present paper may be extended with advantage in the future.

References

[1]Lockwood, F. C., El-Mahallawy, F. M., and Spalding, D. B., "An Experimental and Theoretical Investigation of Turbulent Mixing in a Cylindrical Furnace," *Combustion and Flame,* Vol. 23, 1974, pp. 283-293.

[2]Lilley, D. G., "Flowfield Modelling in Practical Combustors: A Review," *Journal of Energy,* Vol. 3, No. 4, July-Aug. 1979, pp. 193-210.

[3]Elgobashi, S., "Studies in the Prediction of Turbulent Diffusion Flames," *Studies in Convection,* Vol. 2, edited by B. E. Launder, Academic, New York, 1979, pp. 141-189.

[4]Smith, P. J. and Smoot, L. D., "Turbulent Gaseous Combustion, Part II: Theory and Evaluation for Local Properties," *Combustion and Flame,* Vol. 42, 1981, pp. 277-285.

[5]Jones, W. P. and Whitelaw, J. H., "Calculation Methods for Reacting Turbulent Flows: A Reivew," *Combustion and Flame,* Vol. 48, 1982, pp. 1-26.

[6]Vanka, S. P., "Calculation of Axisymmetric Turbulent Confined Diffusion Flames," *AIAA Journal,* Vol. 24, March 1986, pp. 462-469.

[7]Comini, G. and Del Guidice, S., "A (k-ϵ) Model of Turbulent Flow," *Numerical Heat Transfer,* Vol. 8, 1985, pp. 133-147.

[8]Benim, A. C. and Zinser, W., "A Segregated Formulation of Navier-Stokes Equations with Finite Elements," *Computational*

Methods in Applied Mechanics and Engineering, Vol. 57, No. 2, 1986, pp. 223–237.

[9]Brooks, A. N. and Hughes, T. J. R., "Streamline Upwind/Petrov-Galerkin Formulations for Convection Dominated Flows with Particular Emphasis on the Incompressible Navier-Stokes Equations," *Computational Methods in Applied Mechanics and Engineering,* Vol. 32, 1982, pp. 199–259.

[10]Bilger, R. W., "Turbulent Flows with Nonpremixed Reactants," *Turbulent Reacting Flows,* edited by P. A. Libby and F. A. Williams, Springer-Verlag, Berlin, 1980.

[11]Patankar, S. V., *Numerical Heat Transfer and Fluid Flow,* Hemisphere, Washington, DC, 1980.

[12]Chung, T. J., *Finite Element Analysis in Fluid Dynamics,* McGraw-Hill, New York, 1978.

[13]Gresho, P. M., Lee, R. L., and Sani, R. L., "On the Time-Dependent Solution of the Incompressible Navier-Stokes Equations in Two and Three Dimensions," *Recent Advances in Numerical Methods in Fluids,* edited by C. Taylor and K. Morgan, 1980, pp. 27–78.

[14]Launder, B. E. and Spalding, D. B., "The Numerical Computations of Turbulent Flows," *Computer Methods in Applied Mechanics and Engineering,* Vol. 3, 1974, pp. 269–289.

[15]Habib, M. A. and Whitelaw, J. H., "Velocity Characteristics of a Confined Coaxial Jet," *Transactions of the American Society of Mechanical Engineering, Journal of Fluids Engineering,* Vol. 101, 1979, pp. 521–529.